SUPPORTING INFORMATION

Halogen-Bonded Charge-Transfer Co-crystal Scintillators for High-Resolution X-ray Imaging

Yu-Hua Chen,[ab] Guo-Zhen Zhang,[a] Fu-Hai Chen,[a] Shu-Quan Zhang,[c] Xin Fang,[*a] Hong-Ming Chen,[*b] Mei-Jin Lin[*ab]

[a] *Key Laboratory of Advanced Carbon-Based Functional Materials (Fujian Province University), College of Chemistry, Fuzhou University, Fuzhou, 350116, P.R. China. E-mail: meijin_lin@fzu.edu.cn; fangxin@fzu.edu.cn.*

[b] *College of Materials Science and Engineering, Fuzhou University, Fuzhou, 350116, P.R. China. E-mail: chm@fzu.edu.cn.*

[c] *College of Zhicheng, Fuzhou University, Fuzhou, 350002, P.R. China.*

1. Organic synthesis section.

The synthesis of 2,5-dipyridylbithiazole (Py_2TTz) was based on the scheme reported by Alexis N. Woodward *et al.* with suitable adjustments. 4-Pyridinecarboxaldehyde (0.5 mL) and dithiooxamide (0.32 g, 2.67 mmol) was refluxed in anhydrous N,N-dimethylformamide (15 mL) for 6 hours under aerobic conditions. After the reaction, cooled to room temperature and left overnight to precipitate. Filtered, washed with N,N-dimethylformamide and methanol, dried and weighed to get a light yellow solid (350 mg, 44 %). ^{1}H NMR data matched previously reported Py_2TTz.[1]

2. Preparation of Py_2TTz and co-crystallization with I_xF_xB Single crystals.

Py_2TTz (10 mg ,0.03374 mmol) was dissolved in 10 mL of equal proportions of dichloromethane and methanol mixed solvent with heating and stirring, cooled to room temperature, and evaporated slowly for 3 days to obtain light yellow long flaky crystals. Py_2TTz (10 mg ,0.03374 mmol) and equimolar ratios of 1,4-diiodotetrafluorobenzene (I_2F_4B) and 1,3,5-trifluoro-2,4,6-triaiodobenzene (I_3F_3B) was dissolved in 10 mL of equal proportions of dichloromethane and methanol mixed solvent with heating and stirring, respectively, cooled to room temperature, and evaporated slowly for 3 days to obtain light yellow bulk crystals and light yellow rhombic bulk crystals.[2]

3. *Fabrication of photoelectrical devices based on Py_2TTz, Py_2TTz-I_2F_4, and Py_2TTz-I_3F_3 single crystals.*

Py_2TTz with dimensions of 60 × 25 × 5 mm, Py_2TTz-I_2F_4 with dimensions of 40 × 30 × 10 mm, and Py_2TTz-I_3F_3 with dimensions of 80 × 20 × 10 mm single crystals were placed on electronic grade glass with dimensions of 20 × 15 × 0.55 mm, respectively. Then 50 nm thick silver electrodes were deposited onto both ends of the crystals to ensure that the middle part was not short-circuited. Finally, photocurrent testing was performed on a probe stage.

4. *Fabrication of flexible organic scintillator films based on Py_2TTz-I_2F_4.*

A suitable amount of sample was ball milled in poor solvent (water) for about 4 hours. After ball milling, it was dried in an oven and then 25 mg of the powder was dispersed ultrasonically in 5 ml of water. Subsequently, the turbid solution was transferred to another 95 ml of aqueous solution. The dispersion was made step by step. The particle size of the powder after ball milling was measured to be approximately 500 nm. High purity PET polyester microporous filter membranes with a pore size of 0.45 μm and a thickness of 11 μm were selected and placed into a 41 mm sand funnel, and the turbid solution containing the sample was pumped and filtered for 5 hours. Flexible scintillator films with powder adhering to the PET pores were obtained.[3]

5. *Characterization equipment.*

Nuclear Magnetic Resonance (NMR) Hydrogen Spectrum (^{1}H NMR) of the

compounds was tested by a NMR Nuclear Magnetic Resonance Spectrometer from Bruker, Switzerland. Powder X-ray diffraction (PXRD) patterns were measured by a Rigaku MiniFlex-II X-ray diffractometer with Cu-Kα radiation (λ = 1.54184 Å). X-ray diffraction data of Py_2TTz, Py_2TTz-I_2F_4, and Py_2TTz-I_3F_3 were collected by a Rigaku Saturn 724 CCD single-crystal diffractometer at 293 K under a flow of liquid nitrogen from Rigaku Corporation, Japan, and Mo Kα rays (λ = 0.71073 Å) filtered by a graphite monochromator were obtained as the X-ray source. Scintillator performance data were collected on an Edinburgh Instruments Spectrofluorometer FS5. Photoluminescence related data were collected on an Edinburgh Instruments Spectrofluorometer FLS980. The PLQY for crystalline powders were recorded collected by a Horiba FluoroMax-4. The particle size of the powders was measured by NanoPlus3 Zeta potential and nano-particle size analyser.

6. Correlation formulas and analysis methods.

The ESP and the HOMO/LUMO orbitals is based on calculations via Density Functional Theory (DFT) and optimized at the b3lyp/6-31g(d) level. The calculations were run by using the Gaussian09 program. The ESP and the HOMO/LUMO orbitals image visualization was implemented in Multiwfn 3.8 and VMD.

Diffraction data were reduced by the Crystal Clear 1.4.0 structure resolution program with symmetry-dependent data averaging and Lp-factor correction.[4,5] The initial structural model of the crystals was resolved by the SHELXT structure

solving program using the direct method and structure refinement to determine the coordinates of the heavy atoms, then the other non-hydrogen atoms were identified based on the difference Fourier peaks, and anisotropic refinement was applied to all non-hydrogen atoms.[6,7] The coordinates of the hydrogen atoms in the structure are found utilizing a theoretical hydrogenation procedure, and all hydrogen atoms are involved in the structural calculations but not in the structure refinement. The main structural refinement data of the resulting crystals are shown in the table S4.

The X-ray excited relative light yield is calculated as follows:

Attenuation efficiency (T) defines as

$$T = 1 - e^{-\mu_L x} \quad \text{Equation S1}$$

where，x is the effective blocking thickness and μ_L is the linear attenuation coefficient;

$$\frac{\mu_L}{\rho} = \sum_i w_i (\frac{\mu}{\rho})_i \quad \text{Equation S2}$$

where ρ is the density of the material, w_i is the weight fraction of the ith atomic component, $(\frac{\mu}{\rho})_i$ is the mass attenuation coefficient of the ith atom;

The actual light yield of the sample LY_{sample} is defined as

$$LY_{sample} = LY_{standardized} \frac{PC_{sample}}{AE_{smaple}} \Big/ \frac{PC_{standardized}}{AE_{standardized}} \quad \text{Equation S3}$$

where $LY_{standardized}$ is the light yield of the reference, PC (Photon Counting) is the RL spectral integral area of the unknown material, and AE (%) is the attenuation efficiency after pressing.

The detection limit is calculated with reference to Equation S4.

$$LOD = \frac{3\sigma}{slope} \quad \text{Equation S4}$$

where σ is the instrumental average noise and slope is the slope of the fitted line.

Py_2TTz, Py_2TTz-I_2F_4, and Py_2TTz-I_3F_3 single crystal in the solid state were measured by FLS980 under an exciter with 450 nm and the fluorescence decay time is calculated by referring to Equation S5.

$$I(t) = I_0 + A_1 e^{-\frac{t}{\tau_1}} \quad \text{Equation S5}$$

where I(t), I_0 and A_1 are the photoluminescence intensity at time t, background and amplitude, respectively.

The non-radiative transition rate is calculated with reference to Equation S6.

$$k(nr) = \frac{1 - \Phi_f}{\tau_1} \quad \text{Equation S6}$$

where Φ_f is the PLQY and τ is the lifetime.

Calculation of X-ray Imaging Spatial Resolution. X-ray imaging spatial resolution was calculated by Modulation transfer function (MTF) measurements. The photographed line-pair card was imported into the software ImageJ to obtain the curve of pixel intensity versus pixel position, and the MTF was calculated by Equation S7.[8] On this basis, the slanted edge method was used to further calculate

its actual line pairs. Sharp-edge X-ray imaging was performed on a standard line of tungsten sheet with a thickness of approximately 0.5 mm. MTF operation on images through software ImageJ: Then the edge spread function (ESF) was derived from the edge image, and the line spread function (LSF) was derived from the derivation. Finally, the Fourier transform of LSF defined MTF. The MTF function transforms as in Equation S8.[9]

$$MTF = \frac{I_{max} - I_{min}}{I_{max} + I_{min}} \quad \text{Equation S7}$$

where I_{min} and I_{max} are the minimum and maximum values of the function used to quantify the contrast, respectively.

$$MTF(v) = F[LSF(x)] = F\left[\frac{dLSF(x)}{dx}\right] \quad \text{Equation S8}$$

where ν was the spatial frequency and *x* is the position of pixels.

7. *Other related figures.*

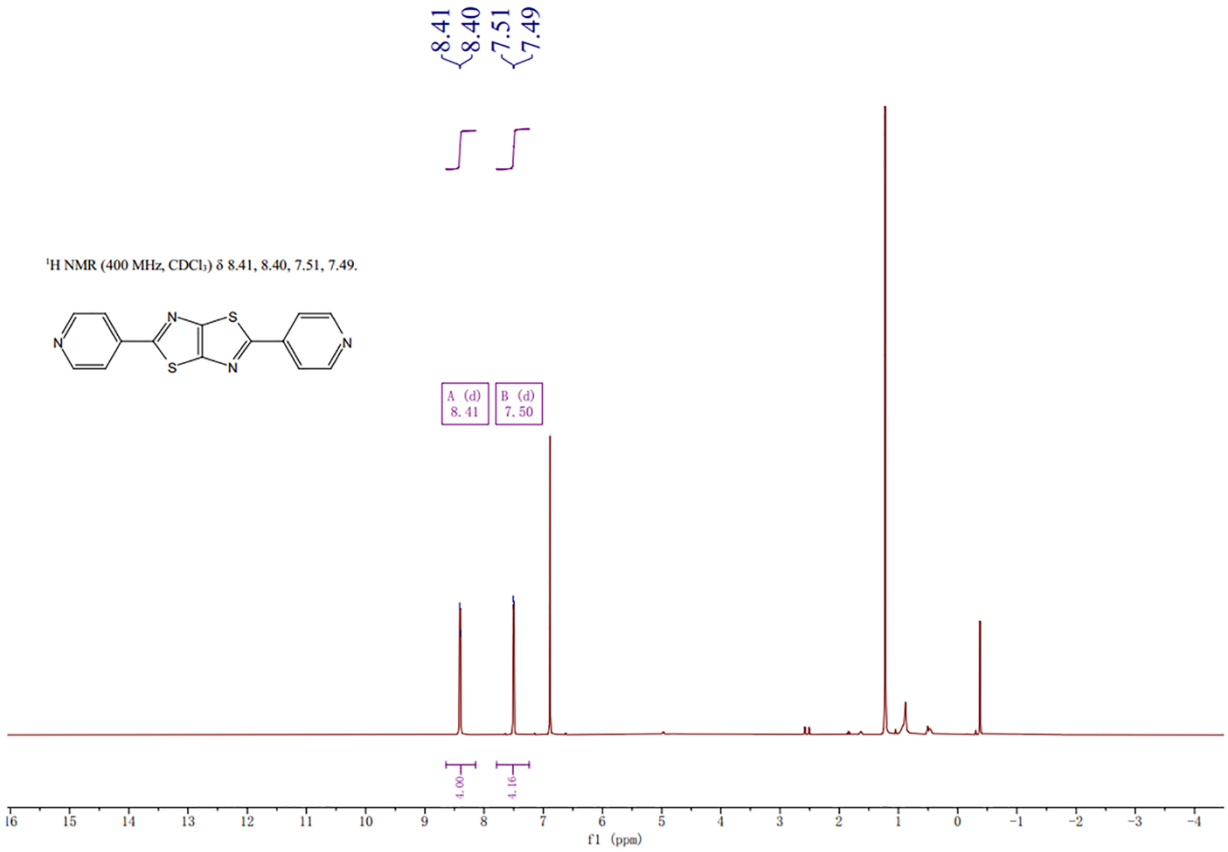

Figure S1. ^{1}H NMR spectrum of compound Py_2TTz in $CDCl_3$.

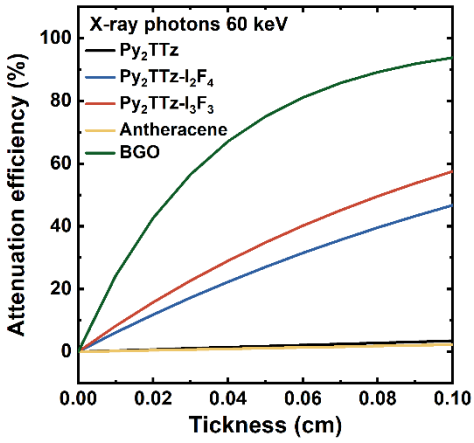

Figure S2. X-ray attenuation efficiency as functions of material thickness for Py_2TTz, Py_2TTz-I_2F_4 and Py_2TTz-I_3F_3.

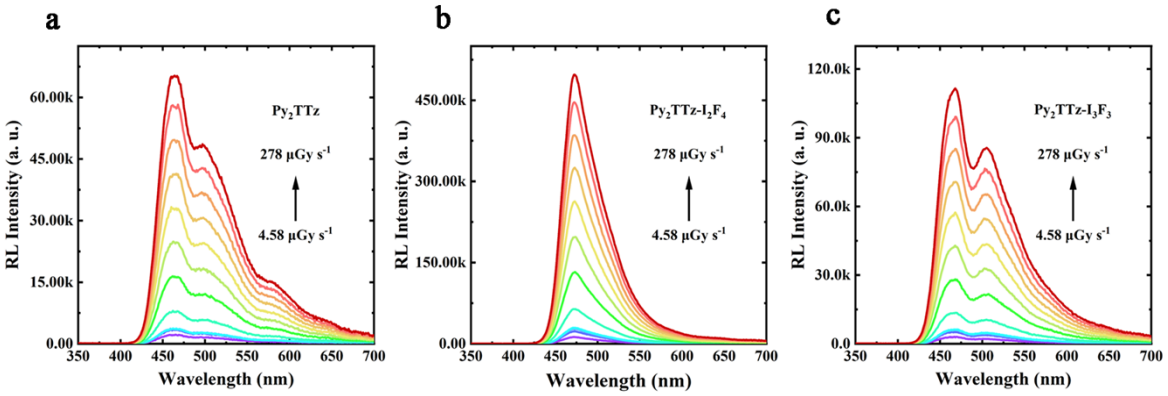

Figure S3. (a)-(c) The RL intensity of Py_2TTz, Py_2TTz-I_2F_4 and Py_2TTz-I_3F_3 crystalline powders under the X-ray dose rates range from 4.58 to 278 μGy s^{-1}, respectively.

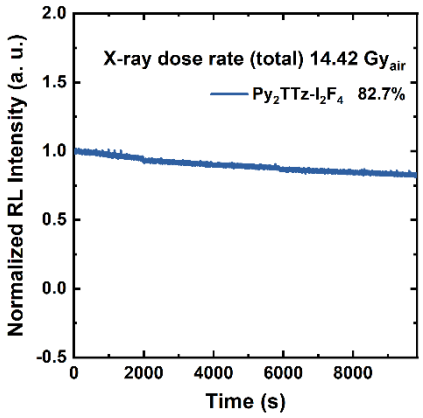

Figure S4. The irradiation stability under continuous irradiation (9832.5 s) for Py_2TTz-I_2F_4 crystals under the X-ray dose rate at 1467 μGy s^{-1}.

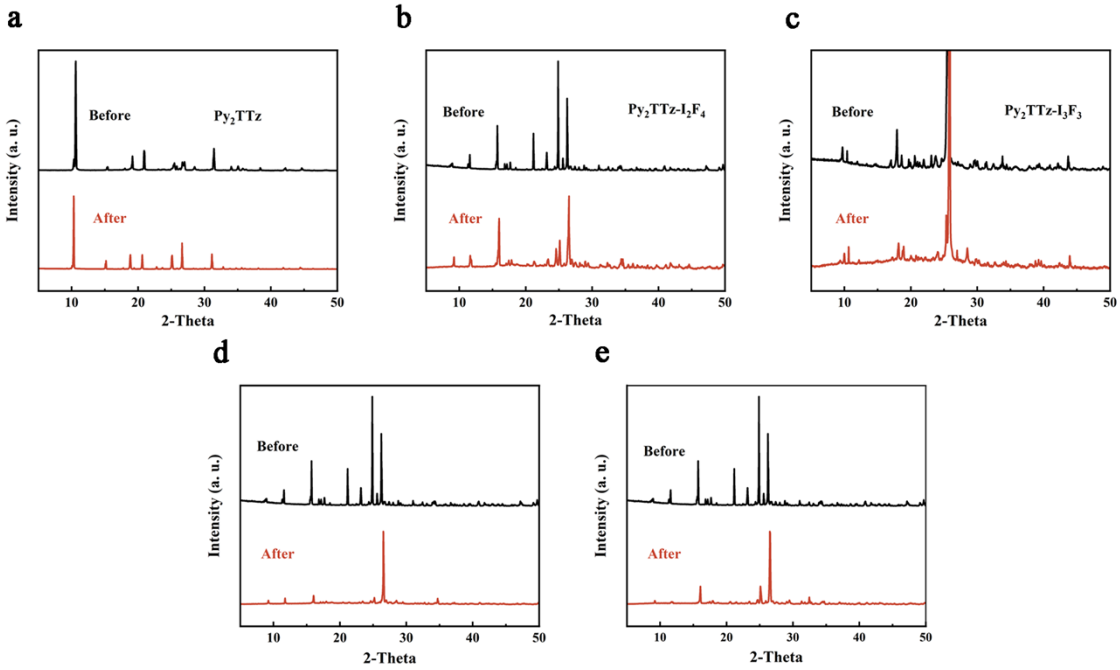

Figure S5. PXRD comparison before and after irradiation. (a) Py_2TTz; (b) Py_2TTz-I_2F_4; (c) Py_2TTz-I_3F_3; (d) 4 days of continuous exposure; (e) Repeat 121 on–off cycles at the X-ray dose rate of 278 μGy s^{-1}.

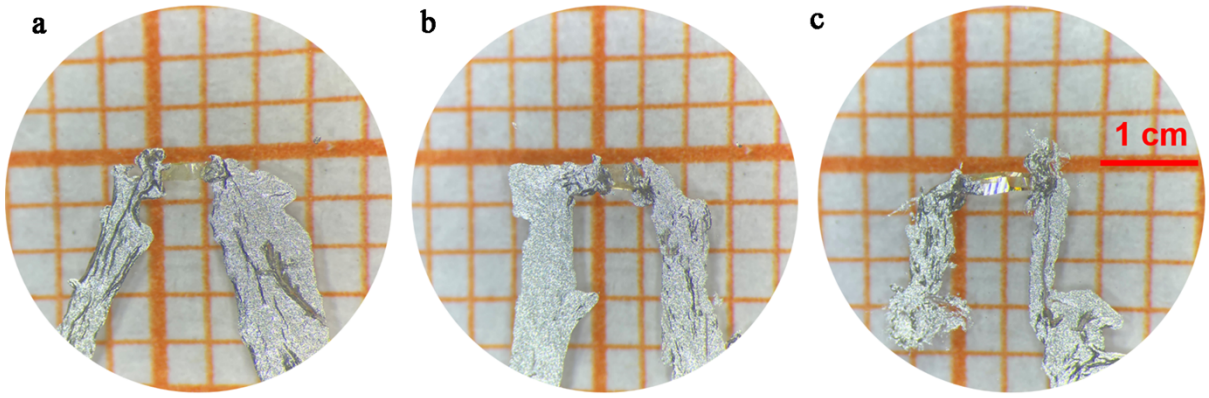

Figure S6. Real photos of photocurrent devices: (a) Py_2TTz; (b) Py_2TTz-I_2F_4; (c) Py_2TTz-I_3F_3. The X-ray irradiated area were respectively (a) 1500 mm^2 (60 × 25); (b) 1200 mm^2 (40 × 30); (c) 1600 mm^2 (80 × 20).

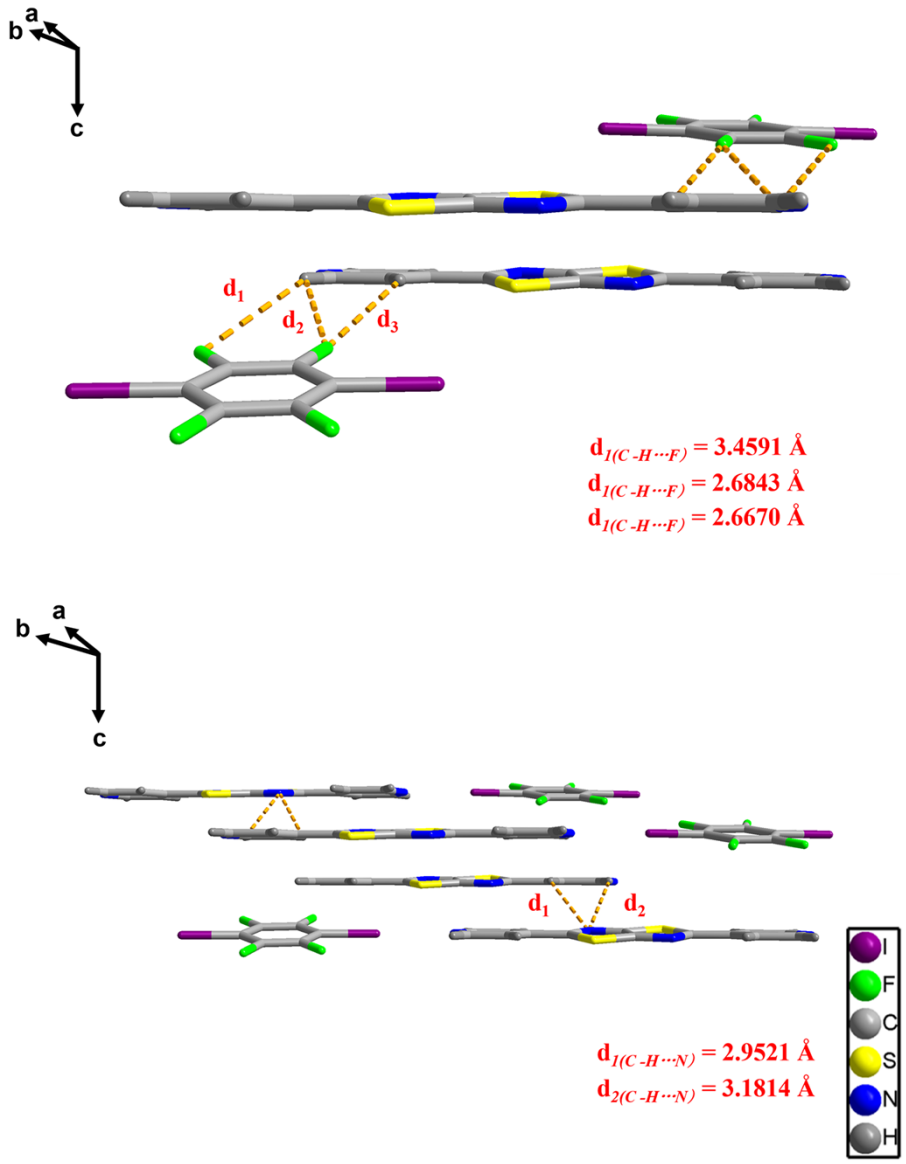

Figure S7. The relevant weak interactions $Py_2TTz\text{-}I_2F_4$.

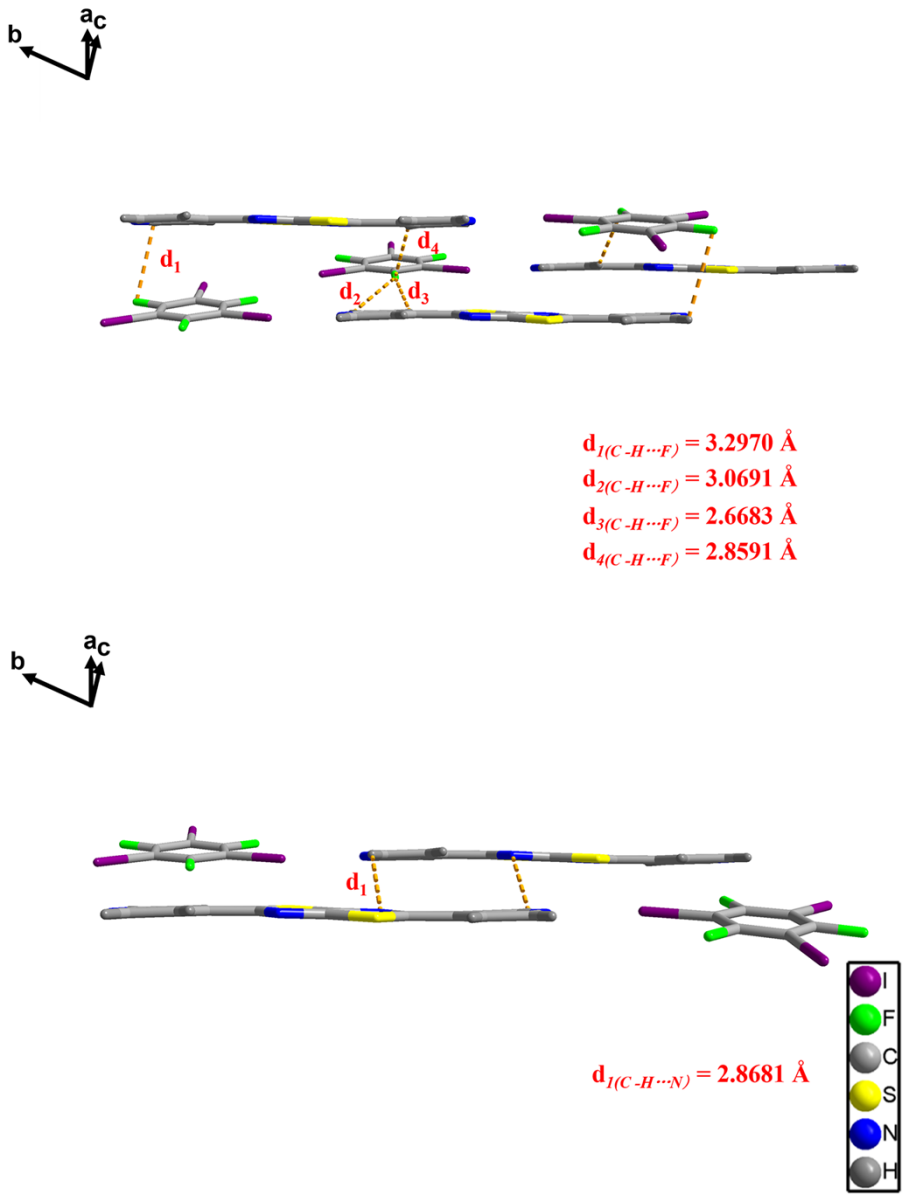

Figure S8. The relevant weak interactions $Py_2TTz\text{-}I_3F_3$.

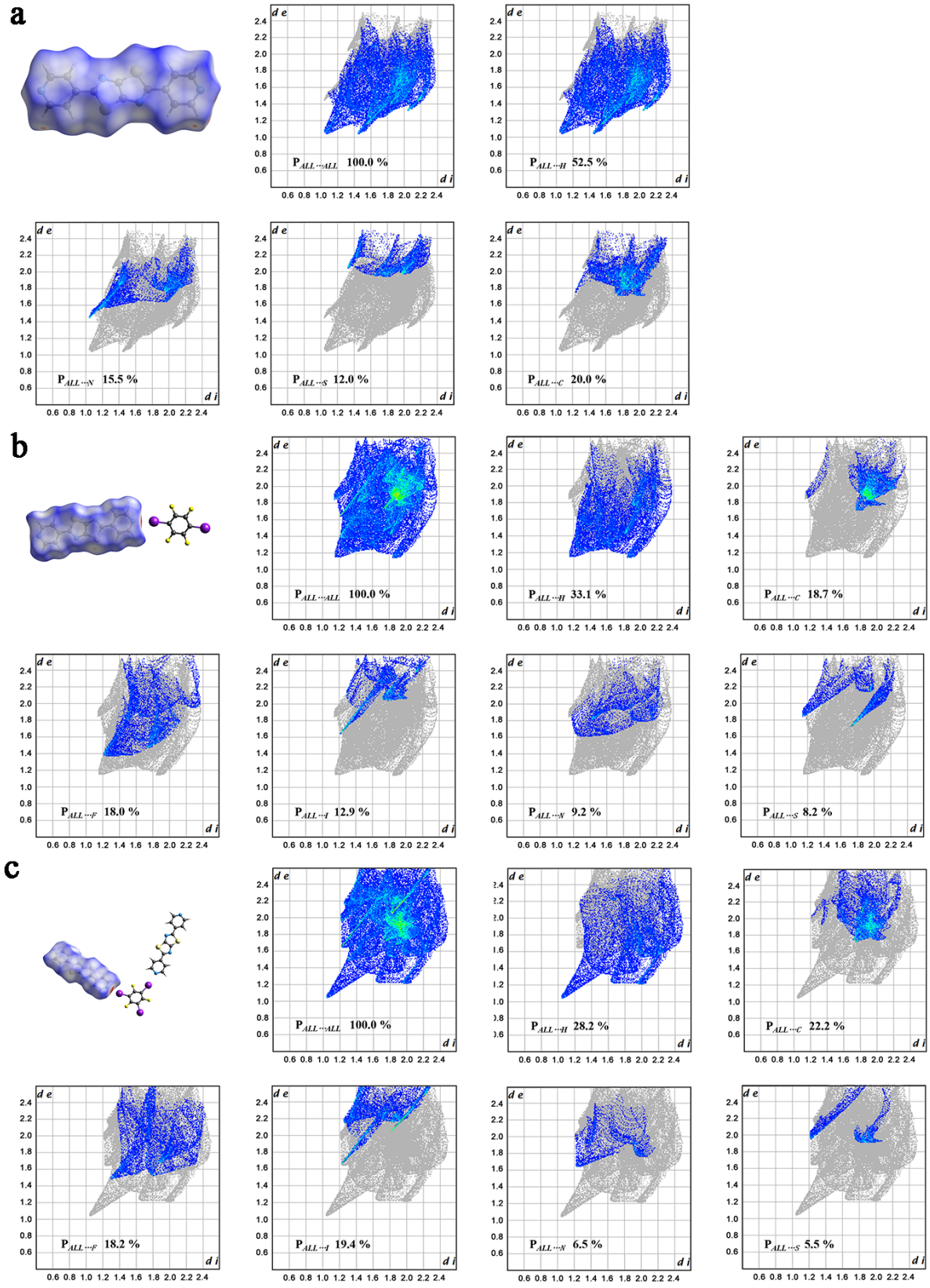

Figure S9. (a)-(c) the Hirshfeld surfaces and the corresponding two-dimensional fingerprint plots of molecules Py_2TTz; Py_2TTz-I_2F_4; Py_2TTz-I_3F_3 mapped with d_{norm} over the range 0.06 to 1.15. Close contacts are shown red on the surfaces.

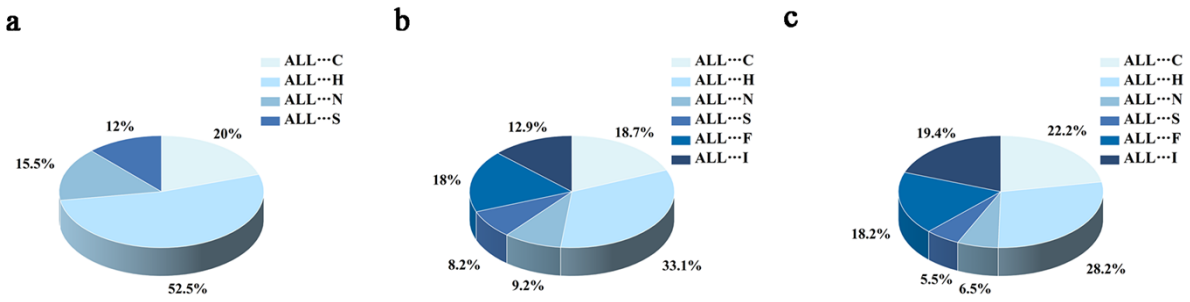

Figure S10. (a)-(c) Relative percentage of various intermolecular interactions (pie charts) of Py_2TTz, Py_2TTz-I_2F_4 and Py_2TTz-I_3F_3.

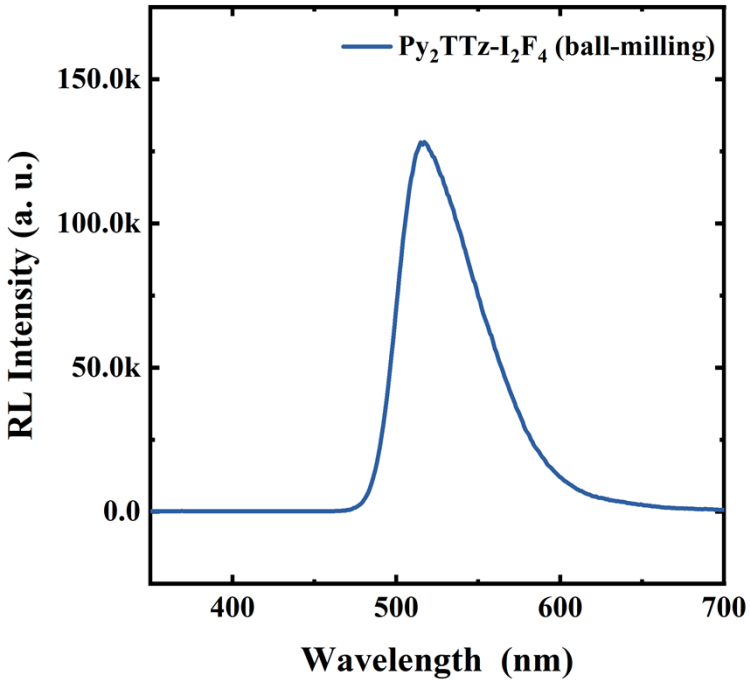

Figure S11. RL spectrum after 4 hours of ball milling.

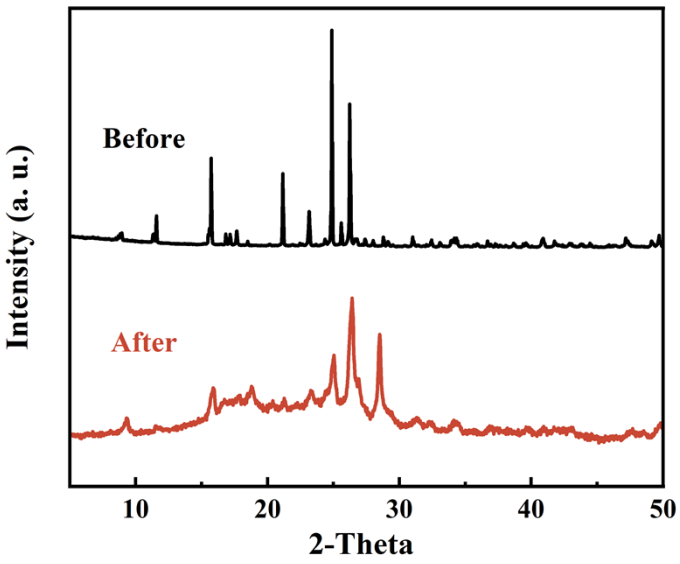

Figure S12. The PXRD comparison of before and after ball milling.

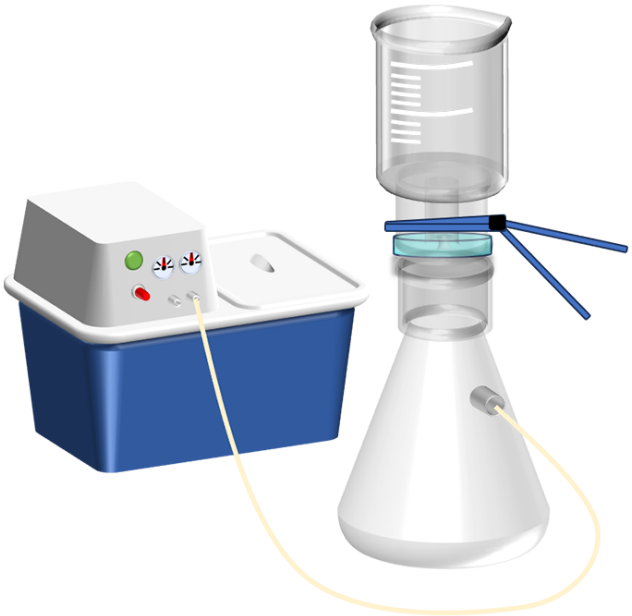

Figure S13. Sand core extraction device.

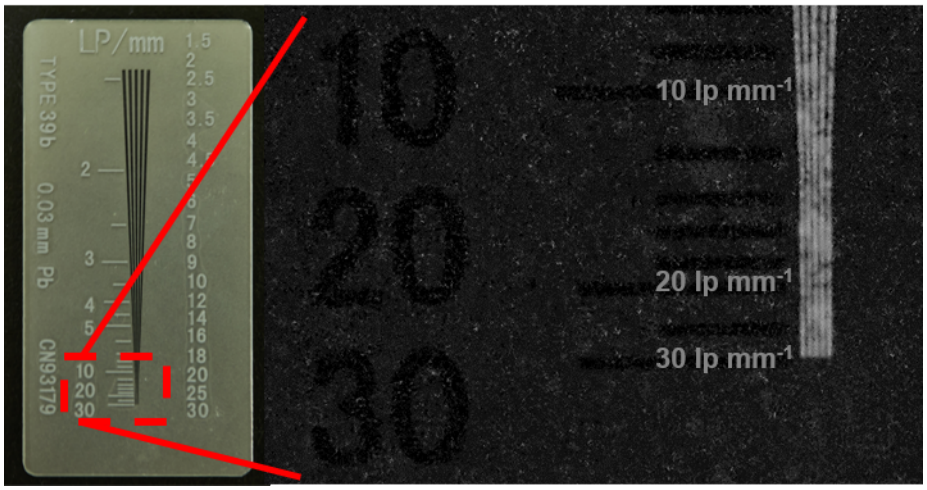

Figure S14. The X-ray exposure contrast images of the line-pair card (Type 39B: 1.5-30 lp mm^{-1})

Table S1. The calculated ESP minimum of Py_2TTz and corresponding spatial locations.

NO.	ESP Minimum (kcal mol^{-1})	Spatial location (Å)		
		x	y	z
1	-34.72	-5.074	6.484	1.718
2	-4.78	-4.257	2.780	-0.331
3	2.12	-2.255	-0.845	1.939
4	-19.43	-1.706	1.888	-2.371
5	-2.70	-1.553	4.698	2.369
6	-3.70	-1.170	5.069	0.929
7	0.65	-1.068	-1.802	-2.427
8	0.65	1.049	1.822	2.443
9	-3.69	1.154	-5.057	-0.918
10	-2.70	1.536	-4.675	-2.397
11	-19.43	1.765	-1.832	2.357
12	2.12	2.273	0.825	-1.949
13	-4.78	4.245	-2.759	0.326
14	-34.71	5.082	-6.480	-1.710

Table S2. The calculated ESP maximum of I_2F_4B and corresponding spatial locations.

NO.	ESP Maximum (kcal mol^{-1})	Spatial location (Å)		
		x	y	z
1	32.34	-5.646	-0.016	-0.017
2	-5.59	-2.137	-3.723	0.028
3	-5.60	-2.174	3.702	-0.030
4	13.11	-0.029	-2.325	1.473
5	15.28	-0.032	-0.031	1.718
6	13.11	-0.029	2.263	-1.528
7	13.13	-0.022	2.293	1.501
8	13.11	0.025	-2.259	-1.500
9	15.26	0.033	-0.039	-1.719
10	-5.60	2.109	-3.739	-0.020
11	-5.59	2.136	3.724	-0.018
12	32.32	5.646	0.037	0.026

Table S3. The calculated ESP maximum of I_3F_3B and corresponding spatial locations.

NO.	ESP Maximum (kcal mol^{-1})	Spatial location (Å)		
		x	y	Z
1	-5.46	-4.138	1.143	-0.018
2	30.38	-3.986	-4.007	-0.019
3	12.38	-1.914	0.523	-1.750
4	12.37	-1.908	0.543	1.749
5	30.38	-1.467	5.458	-0.018
6	12.77	-0.032	0.037	1.722
7	12.77	0.027	0.027	-1.721
8	12.37	0.534	-1.920	-1.746
9	12.38	0.479	-1.911	1.755
10	-5.46	1.091	-4.152	-0.018
11	12.36	1.404	1.388	-1.753
12	12.38	1.372	1.421	1.754
13	-5.46	3.029	3.042	0.028
14	30.38	5.460	-1.459	-0.019

Table S4. Crystal datum and structure refinement parameters for Py_2TTz, Py_2TTz-I_2F_4 and Py_2TTz-I_3F_3

Complex	**Py_2TTz**	**Py_2TTz-I_2F_4**	**Py_2TTz-I_3F_3**
Empirical formula	$C_{14}H_8N_4S_2$	$C_{20}H_8F_4I_2N_4S_2$	$C_{20}N_4I_3F_3S_2H_8$
Formula weight	296.36	698.22	806.12
Temperature/K	296.15	296.15	296.15
Crystal system	monoclinic	triclinic	triclinic
Space group	*P2$_1$/c*	*P-1*	*P-1*
a/Å	8.6682(13)	6.2882(4)	7.7556(5)
b/Å	6.2486(8)	8.7402(4)	8.7408(6)
c/Å	11.8011(17)	11.0715(5)	18.7834(12)
α/°	90	106.876(4)	84.004(5)
β/°	93.515(13)	102.839(5)	79.941(5)
γ/°	90	105.122(5)	67.184(6)
Volume/Å^3	637.99(16)	532.08(5)	1154.71(14)
Z	2	1	2
ρcalcg/cm^3	1.543	2.179	2.319
μ/mm^{-1}	0.410	3.203	4.282
F(000)	304.0	330.0	748.0
Crystal size/mm^3	0.2 × 0.05 × 0.02	0.01 × 0.01 × 0.01	0.02 × 0.05 × 0.02
Radiation		Mo Kα (λ = 0.71073)	
2Θ range for data collection/°	4.708 to 58.558	4.062 to 58.784	4.408 to 58.752
Index ranges	-9 ≤ h ≤ 11, -8 ≤ k ≤ 7, -12 ≤ l ≤ 15	-7 ≤ h ≤ 7, -11 ≤ k ≤ 11, -12 ≤ l ≤ 15	-10 ≤ h ≤ 10, -11 ≤ k ≤ 11, -24 ≤ l ≤ 25
Reflections collected	4982 1462	7427 2434	17322 5256
Independent reflections	[Rint = 0.0615, Rsigma = 0.0786]	[Rint = 0.0533, Rsigma = 0.0414]	[Rint = 0.0373, Rsigma = 0.0371]
Data/restraints/parameters	1462/0/91	2434/6/145	5256/0/290
Goodness-of-fit on F^2	1.049	1.006	1.060
R_1[a], wR_2[b] [I>=2σ (I)]	R_1 = 0.0497, wR_2 = 0.1091	R_1 = 0.0248, wR_2 = 0.0485	R_1 = 0.0280, wR_2 = 0.0575
R_1[a], wR_2[b] [all data]	R_1 = 0.0814, wR_2 = 0.1229	R_1 = 0.0303, wR_2 = 0.0498	R_1 = 0.0426, wR_2 = 0.0612
Largest diff. peak/hole / e Å^{-3}	0.27/-0.26	0.51/-0.91	0.84/-0.65

[a] $R_1 = \sum||F_0| - |F_c||/\sum|F_0|$, [b] $wR_2 = [\sum w(F_0^2 - F_c^2)^2 / \sum w(F_0^2)]^{1/2}$.

Table S5. The X-ray dose rate versus voltage/current.

Current (μA)	Voltage (kV)	Dose rate (μGy s^{-1})
5	20	4.58
5	30	9.64
5	40	11.91
5	50	17.38
10	50	34.57
20	50	69.50
30	50	104.25
40	50	139.00
50	50	173.75
60	50	208.50
70	50	243.35
80	50	278.00

Table S6. Decay time, PLQY and non-radiative transition rates calculation of Py_2TTz, Py_2TTz-I_2F_4 and Py_2TTz-I_3F_3 crystalline powders.

Materials	A_1	τ_1 (ns)	R^2	Φ_f	$k_{(nr)}(s^{-1})$
Py_2TTz	136.401	0.913	0.996	12.09%	9.63×10^8
Py_2TTz-I_2F_4	23.911	1.426	0.996	18.85%	5.69×10^8
Py_2TTz-I_3F_3	97.331	0.998	0.996	15.92%	8.42×10^8

Table S7. Summary of scintillation properties for Py_2TTz, Py_2TTz-I_2F_4 and Py_2TTz-I_3F_3 as compared with anthracene and $Bi_4Ge_3O_{12}$ (BGO).

Materials	Maxiumum emission (nm)	FWHM (nm)	RL intensity	Detection limit (μGy s^{-1})	Decay time (ns)
Py_2TTz	464	87	65335	508.29	0.913
Py_2TTz-I_2F_4	472	52	497207	70.49	1.426
Py_2TTz-I_3F_3	468	88	111575	313.94	0.998
Antherance	455,508,542	36,18,28	177786	506.0	8.30
BGO	500	137	340055	/	~300

Table S8. Comparative Analysis of Stability Testing Conditions for Organic Scintillators in X-ray Imaging Literature.

Materials	Stability	Irradiation time	X-ray dose rate
9,10-DPA	94%	233 cycles over 174 days	-
DMAc-TRZ	Nearly unchanged	-	3.034 mGy s^{-1}
O-ITC	94%	1800 s	278 μGy s^{-1}
BIC	93%	166 cycles over 10000 s	34.75 μGy s^{-1}
PNP-A	Nearly unchanged	1800 s	120 μGy s^{-1}
CBP	99.2%	1800 s	278 μGy s^{-1}
BPA-Br	98.5%	1800 s	278 μGy s^{-1}
$Py_2TTz\text{-}I_2F_4$	98.9%	1800 s	278 μGy s^{-1}

Reference

1 A. N. Woodward, J. M. Kolesar, S. R. Hall, N. A. Saleh, D. S. Jones and M. G. Walter, *J. Am. Chem. Soc.*, 2017, **139**, 8467-8473.

2 M. Ghora, P. Majumdar, M. Anas and S. Varghese, *Chem. Eur. J.*, 2020, **26**, 14488-14495.

3 H. Chen, M. Lin, Y. Zhu, D. Zhang, J. Chen, Q. Wei, S. Yuan, Y. Liao, F. Chen, Y. Chen, M. Lin and X. Fang, *Small*, 2023, 2307277.

4 A. Spek, *J. Appl. Crystallogr.*, 2003, **36**, 7-13.

5 L. Farrugia, *J. Appl. Crystallogr.*, 2012, **45**, 849-854.

6 G. Sheldrick, *Acta Crystallogr., Sect. A: Found. Crystallogr.*, 2015, **71**, 3-8.

7 G. Sheldrick, *Acta Crystallogr., Sect. C: Cryst. Struct. Commun.*, 2015, **71**, 3-8.

8 H. Chen, M. Lin, C. Zhao, D. Zhang, Y. Zhang, F. Chen, Y. Chen, X. Fang, Q. Liao, H. Meng and M. Lin, *Adv. Opt. Mater.*, 2023, **11**, 2300365.

9 H. Zhang, C. Li and Y. Duan, *Optik*, 2018, **157**, 635-643.